

Efficient interfacing of fluid and structure for aeroelastic instability predictions

Nesrin Sarigul-Klijn*

Department of Mechanical and Aeronautical Engineering, University of California at Davis, Davis, CA 95616-5294, U.S.A.

SUMMARY

An efficient procedure for multidisciplinary computation of fluid and structure interaction problems of aerospace vehicles is presented. It features the use of Meshless Methods, Finite Elements, Rayleigh–Ritz, and Kernel Functions enabling the aeroelastic requirements to be included in design without demanding prohibitive computational efforts. Improvements made are in terms of choosing meshless fluid–structure interface for displacement and aerodynamic load transfer, including nine modes in Rayleigh–Ritz, introducing Gradient Adaptive Transfinite Element in Finite Element model, and taking into account deformations of structure in aerodynamic load calculations. Numerical results are presented for flutter and divergence type aeroelastic responses of lifting surfaces constructed of advanced composites and super alloys at subsonic, supersonic, and hypersonic flight velocities. Copyright © 2000 John Wiley & Sons, Ltd.

KEY WORDS: meshless methods; finite elements; Rayleigh–Ritz; Kernel methods; composites; aerodynamic heating

INTRODUCTION

One of the most critical of multidisciplinary activities in aircraft, reusable launch vehicle, and aerospace plane design is aeroelastic instability predictions and avoidance. Aeroelasticity combines the disciplines of structural analysis, structural dynamics, steady and unsteady aerodynamics as a result of the interaction between aerodynamic forces and the deformations induced thereby in the structure of a flight vehicle [1, 2]. For flight vehicles at high velocities aerothermoelastic loads become critical due to aerodynamic heating [3–5]. In order to achieve desired minimum weight design of flight vehicles, the aeroelastic instabilities, such as flutter and divergence of lifting surfaces, must be included before the initial flight tests. ‘Aeroelastic fixes’ for flutter, for example, at a later stage in design always result in added weight to the vehicle penalizing its performance and increasing its operational cost in addition to increasing initial cost.

In this paper an efficient approach for aeroelastic analysis, namely flutter and divergence, that is suitable to be integrated in the design stage of aerospace vehicles is presented. This approach couples Finite Element Method [6], Rayleigh–Ritz [1], Kernel Functions and Meshless Methods

*Correspondence to: Nesrin Sarigul-Klijn, Department of Mechanical and Aeronautical Engineering, University of California at Davis, Davis, CA 95616-5294, U.S.A. E-mail: nsarigulklijn@ucdavis.edu

[7]. Numerical examples include composite lifting surfaces at subsonic, supersonic, and hypersonic velocities. Numerical results for various cases are obtained using the author's research computer program in Fortran called AIM (Aeroelastic Instability Modes) [8]. Fluid and structure are interfaced using meshless methods. Since structure and aerodynamic disciplines are interfaced it is easier to incorporate the latest technical capabilities from each discipline. As an example, Computational Fluid Dynamic codes which incorporate various levels of complexity in the model equations of the fluid, from linear theory through full Navier–Stokes, can be incorporated in the system through development of common or similar interfaces without modification to the aeroelastic codes. This assures that the latest version will be available to the multidisciplinary analysis in a transparent manner. For example, with the applications presented here using AIM code, the structure modelling incorporated a recent development in Finite Elements based on Boolean sum [9] as well as the Rayleigh–Ritz method.

In practical applications, the requirements to generate the discretized models of the fluid and structure are subjected to different constraints. Developments based on spline curves goes back to mid-sixties [10]. Studies based on full Navier–Stokes are costly.

Here, a meshless approach is introduced to solve the fluid and structure interaction problem. Meshless methods have been applied to many problems in mechanics. An excellent overview is given in [7]. In meshless methods the approximating function is described in terms of nodes and a domain geometry. Three-dimensional deformations of the structure and the aerodynamic loads are transferred using nodes. Structural deformations are taken into account in aerodynamic load calculations. Numerical results for subsonic, supersonic, and hypersonic flight velocities are given for isotropic and composite lifting surfaces. Results are found to be in good agreement with experimental predictions when available and against each other. Structural model and displacement verifications are also conducted by using ABAQUS commercial code [11]. New results are also presented for flight at high velocities including aerodynamic heating effects.

PROBLEM FORMULATION AND BASIC ASSUMPTIONS

The fluid and structure interaction problem to be considered is schematically shown in Figure 1 for 3-D and in Figure 2 for 2-D. The structure is idealized by using either the equivalent plate or full three-dimensional built-up of complex construction of the lifting surface, and the fluid domain is modelled by using unsteady aerodynamics taking into account subsonic, supersonic, and hypersonic velocities of flight. Fluid loads, in this case the aerodynamic loads, are calculated by using the oscillations of the lifting surface. Communication between the fluid and the structure are accomplished through the meshless approach.

The structure region (S) simulated by using either Rayleigh–Ritz or Finite Elements. When Finite Element method is used the elements are taken from the Gradient Adaptive Transfinite Elements (GATE) family. These elements are developed by using transfinite interpolates and the Boolean sum.

In deriving equations of equilibrium for aeroelasticity, we refer to Hamilton's principle written for non-conservative system as follows:

$$\int_{t_1}^{t_2} \delta(T - V) dt + \int_{t_1}^{t_2} \delta W_{nc} dt = 0 \quad (1)$$

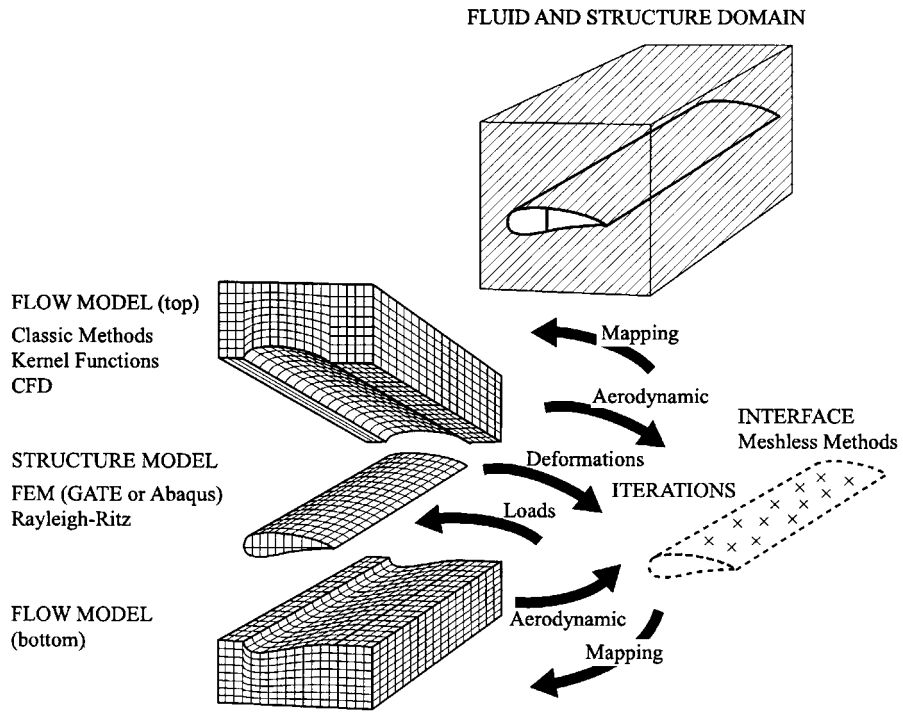


Figure 1. Fluid and structure interaction in 3-D

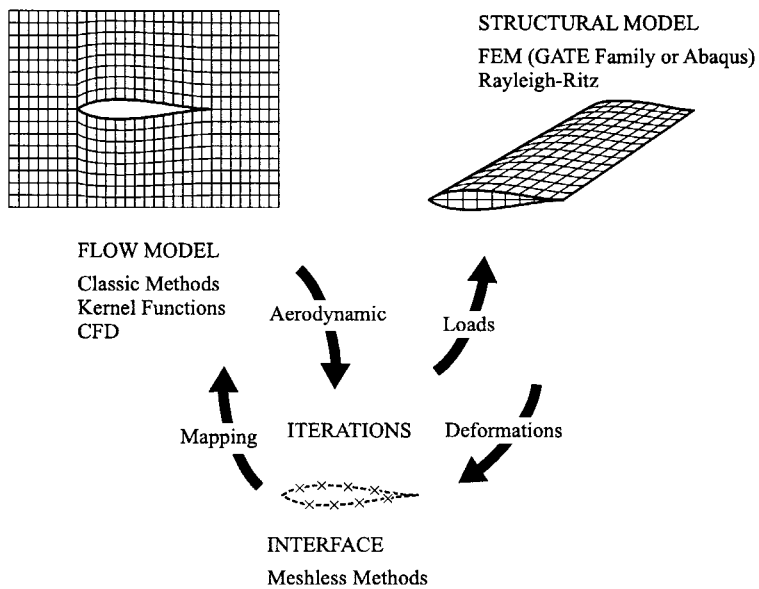


Figure 2. Lifting surface structure and flow in 2-D

where T represents the instantaneous kinetic energy measured relative to any inertial set of coordinates, and U is the potential energy of the system including the strain energy, and the potential energy of conservative external forces. δW_{nc} is the virtual work done by non-conservative forces including damping forces and external forces not accounted for in V . δ is the variational symbol, t_1 and t_2 are the times at which the configuration of the system is known.

Of all admissible displacements between specified initial and final conditions at times t_1 and t_2 which satisfy the prescribed displacement boundary conditions of the system, the displacements which also satisfy equilibrium and the stress boundary conditions are selected by the extremum principle.

The Euler differential equations of the above equation are the equations of equilibrium of the system. In addition, the stress boundary conditions are produced as a by-product.

A continuous system can be envisioned as an infinite number of degrees of freedom system. In most aeroelastic applications the structure usually is approximated to have only a finite number of independent degrees of freedom. This means that there are n generalized co-ordinates $q_1(t), q_2(t), \dots, q_n(t)$ such that the structural displacements are completely known once the $q_i(t)$ is specified. For an n degrees of freedom system the generalized co-ordinates are defined as any set of independent quantities which are sufficient to completely specify the position of every point within the system.

For most mechanical and structural systems the kinetic energy can be expressed in terms of the generalized co-ordinates and their first time derivatives, and the potential energy can be expressed in terms of generalized co-ordinates. In addition, the virtual work of non-conservative forces as they act through virtual displacements caused by arbitrary variations in the generalized co-ordinates can be expressed as a linear function of those variations. Therefore

$$T = T(q_1, q_2, \dots, q_n, \dot{q}_1, \dot{q}_2, \dots, \dot{q}_n, t) \quad (2)$$

$$V = V(q_1, q_2, q_3, \dots, q_n, t) \quad (3)$$

$$\delta W_{nc} = Q_1 \delta q_1 + Q_2 \delta q_2 + \dots + Q_n \delta q_n \quad (4)$$

where Q_1, Q_2, \dots, Q_n are called the generalized forces, and each term $Q_i \delta q_i$ has the units of work.

Hamilton's principle

$$\int_{t_1}^{t_2} \delta(T - V) dt + \int_{t_1}^{t_2} \delta W_{nc} dt = \int_{t_1}^{t_2} \sum_{i=1}^n \left\{ \frac{\delta T}{\delta \dot{q}_i} \delta \dot{q}_i + \left[\frac{\partial(T - V)}{\partial q_i} + Q_i \right] \delta q_i \right\} dt = 0 \quad (1a)$$

An integration by parts with respect to time of the first term with considerations of $\delta q_i = 0$ at time t_1 and t_2 since the state of the system is specified leads to

$$\int_{t_1}^{t_2} \sum_{i=1}^n \left[-\frac{d}{dt} \left(\frac{\delta T}{\delta \dot{q}_i} \right) + \frac{\partial(T - V)}{\partial q_i} + Q_i \right] \delta q_i dt = 0 \quad (1b)$$

Since the variations of the independent co-ordinates q_i may be chosen arbitrarily, the terms inside the brackets must vanish resulting in n differential equations of the form, Lagrange's equation of motion

$$\frac{d}{dt} \left(\frac{\partial T}{\partial \dot{q}_i} \right) - \frac{\partial T}{\partial q_i} + \frac{\partial V}{\partial q_i} = Q_i \quad i = 1, \dots, n \quad (5)$$

these equations are valid for non-linear systems as well as linear systems.

They generate both the exact equations for lumped parameter systems and approximate representations to any desired degree of accuracy for continuous or distributed parameter systems. These equations form the basis for the useful approximation technique Rayleigh–Ritz method, a modal method.

The governing aeroelastic equations of motion of a flexible lifting surface are solved using the Rayleigh–Ritz method. There are some attractive reasons for using the modal approach. In this method the resulting aeroelastic displacements at any time are expressed as a function of a set of assumed modes. The contribution of each mode to the total motion is derived by using Lagrange's equation. Furthermore, it is assumed that the deformation at the continuous lifting surface can be represented by deflections at a set of discrete points. This assumption facilitates the use of discrete structural data, such as modal vector, the modal stiffness matrix, the modal mass matrix, and the aerodynamic matrix. These can be generated from experimental or analytical methods. In this study the Finite Element method and Rayleigh–Ritz method are used for the structural modal matrix computations; modified Kernel functions methods that take into account the deformations of the structure is used [12]. The final matrix form of the aeroelastic equations of motion is

$$[M]\{\ddot{q}\} + [G]\{\dot{q}\} + [K]\{q\} = \{Q\} \quad (6)$$

where $[M]$, $[G]$ and $[K]$ are modal mass, damping and stiffness matrices, respectively. $\{Q\}$ is the aerodynamic load vector.

If the structure is rotating, then the stiffness matrix contains the centrifugal force terms and the damping matrix contains Coriolis terms in addition to viscous damping terms. Depending on the type of aeroelastic instability sought, various forms of equation (6) can be obtained. Solution methods to flutter and divergence type aeroelastic instability equations are detailed in the following section.

SOLUTION OF AEROELASTIC EQUATIONS

In this paper two types of aeroelastic instabilities are studied, flutter and divergence. Assuming harmonic motion, the generalized displacements can be expressed as

$$q = \bar{q}e^{i\omega t}, \quad \dot{q} = i\omega\bar{q}e^{i\omega t}, \quad \ddot{q} = -\omega^2\bar{q}e^{i\omega t} \quad (7)$$

where ω is the frequency. The equation of motion for flutter analysis, neglecting structural damping and using equation (6) and (7) becomes

$$([K] - \omega^2[B])\{\bar{q}\} = 0 \quad \text{with} \quad [B] = [M] + [A] \quad (8)$$

$[B]$ matrix is complex due to complex aerodynamic terms. For flutter type instabilities equation (8) is solved. Among the various solution techniques, the $U-g$ method is used in this research.

In the $U-g$ method structural damping is introduced by multiplying the structural frequencies squared (ω_n^2, ω_x^2) by $(1 + ig)$ where g is an artificial structural damping coefficient and pure sinusoidal motion is assumed, i.e. $\omega = \omega_R$ with $\omega_I = 0$, with ω_R being the real and ω_I being the imaginary parts of the frequency.

For a given U the g is required to sustain pure sinusoidal motion for each aeroelastic mode determined. The computational advantage of this approach is that the aerodynamic forces only need be determined for real frequencies. The disadvantage is the loss of physical insight. For example, if a system (with no structural damping) is stable at a given airspeed, U , all the values of g so determined will be negative, but these values of g cannot be interpreted directly in terms of ω_I . Moreover, for a given system with some prescribed damping, only at one airspeed $U = U_F$ (where $\omega = \omega_R$ and $\omega_I \equiv 0$) will the mathematical solution be physically meaningful. The limitations of the $U-g$ method are fully appreciated by experienced practitioners and it is a measure of the difficulty of determining the aerodynamic forces for other-than pure sinusoidal motion that this method remains popular. The usual definition of reduced frequency is introduced in terms of the half chord b of the lifting surface, flow velocity, and frequency

$$k = \omega b/U \quad (9)$$

The $U-g$ method flutter analysis leads to the following eigenvalue equation at the airspeed associated with neutral stability (flutter):

$$[[B] - \lambda[K]]\{\bar{q}\} = \{0\} \quad (10)$$

where $[B]$ is a generalized complex matrix, λ the eigenvalue, and $\{\bar{q}\}$ the eigenvector. The eigenvalue λ is defined as $\lambda = (1 + ig)/\omega^2$ and the generalized complex matrix $[B]$ is defined as

$$[B] = [[M] + [A]] \quad (11)$$

where $[K]$ and $[M]$ are the stiffness and mass matrix $[A]$ is the aerodynamic matrix and g is the artificial damping coefficient introduced in $U-g$ method.

The complex eigenvalue problem shown in equation (8) is solved for U and g values by using a wide range of reduced frequencies. Flutter velocities and modes are then identified.

In case of divergence instability predictions the mass matrix and the time-dependent terms of aerodynamic matrix is equated to zero in equation (6). The equation of motion and the corresponding eigenvalue problem take the form given below:

$$[[A_{\text{real}}] - \bar{\lambda}[K]]\{\bar{q}\} = \{0\} \quad (12)$$

where $[A_{\text{real}}]$ aerodynamic matrix contains real terms and $\bar{\lambda} = 1/U^2$. The largest positive eigenvalue yields the divergence speed of the lifting surface.

STRUCTURE MODEL AND SOLUTION METHODS

Both Rayleigh–Ritz and Finite Element methods are used in modelling the lifting surface, either as equivalent thin plate or as a three-dimensional built-up structure.

The lifting surface is idealized as either isotropic material or laminated composite equivalent thin plate in two-dimensional flow in the direction of negative y -axis as depicted in Figure 3.

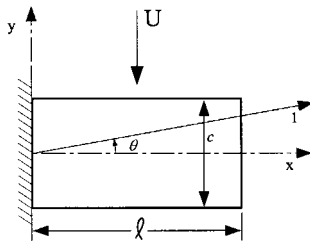


Figure 3. Composite lifting surface

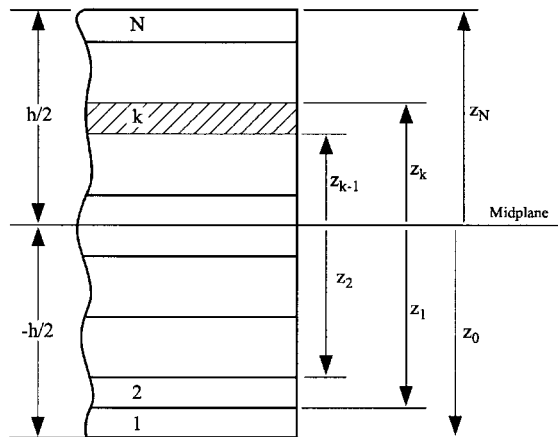


Figure 4. Ply stacking sequence

In a multi-layer fiber composite lifting surface the displacements through the thickness, h , cannot typically be expressed by a simple function, Figure 4. In order to achieve a general representation, the displacements are initially expressed by a power series expansion in z direction for an equivalent plate lifting model which takes the form

$$u = \sum_{i=0}^{\infty} z^i \Phi(x, y), \quad v = \sum_{i=0}^{\infty} z^i \Psi(x, y), \quad \zeta = \sum_{i=0}^{\infty} z^i \Theta(x, y) \tag{13}$$

The number of series terms retained as well as assumptions made with regard to permissible strain fields dictate the form of Φ , Ψ and Θ . For thin plates subject to small deformations, which is the case in this study, Kirchhoff hypothesis is valid:

- (1) The deflections of mid-surface are small compared to the thickness of the plate. Therefore, the slope of the deflected plate is small.
- (2) The mid-plate is unstrained subsequent to pure bending.
- (3) Plane sections initially normal to the mid-plane remain normal to the mid-plane after bending. Therefore, shear strains components γ_{xz} and γ_{yz} are assumed to be negligible.

Similarly, normal strains out of plane are assumed to be zero when deflections are due to bending.

- (4) Conditions of ($\sigma_z = 0$) is assumed to be valid, except in localization areas where high concentrations of transverse load are applied.

In the case of thin, laminated plates, the total laminate thickness is usually small when compared to the other plate dimensions. Therefore, a good approximation is achieved by retaining only the first few terms of u and v from the series identified above, as follows:

$$u = u_0(x, y) + z\Phi(x, y) \quad (14)$$

$$v = v_0(x, y) + z\Psi(x, y) \quad (15)$$

$$\zeta = w_0(x, y) \quad (16)$$

By using these displacement equations, strain can be expressed as

$$\begin{Bmatrix} \varepsilon_x \\ \varepsilon_y \\ \varepsilon_{xy} \end{Bmatrix} = \begin{Bmatrix} \varepsilon_x^0 \\ \varepsilon_y^0 \\ \varepsilon_{xy}^0 \end{Bmatrix} + z \begin{Bmatrix} \kappa_x \\ \kappa_y \\ \kappa_{xy} \end{Bmatrix} \quad (17)$$

The lifting surface is modelled as a multi-layered composite laminate plate as described by Jones [13]. The internal forces $\{N\}$ and the moments $\{M\}$ are the result of the unsteady aerodynamic loads and are related to extension and flexure of the plates as

$$\begin{Bmatrix} \{N\} \\ \{M\} \end{Bmatrix} = \begin{bmatrix} [A] & [B] \\ [B] & [D] \end{bmatrix} \begin{Bmatrix} \{\varepsilon\} \\ \{\kappa\} \end{Bmatrix} \quad (18)$$

where the matrices $[A]$, $[B]$, and $[D]$ are the extensional, extension–bending coupling, and bending stiffness matrices, respectively. The term $\{\varepsilon\}$ represents mid-surface strains and $\{\kappa\}$ represents the curvature.

The stiffness of each lamina in the principal material direction is defined as

$$[Q] = \begin{bmatrix} \frac{E_{11}}{1 - v_{12}v_{21}} & \frac{v_{12}E_{22}}{1 - v_{12}v_{21}} & 0 \\ \frac{v_{12}E_{22}}{1 - v_{12}v_{21}} & \frac{E_{22}}{1 - v_{12}v_{21}} & 0 \\ 0 & 0 & G_{12} \end{bmatrix} \quad (19)$$

where E_{11} , E_{22} , v_{12} , G_{12} , and v_{21} are constitutive properties of the lamina. The subscript 1 indicates the fibre direction and the subscript 2 indicates the direction perpendicular to the fibre direction. These directions are related to the (x, y, z) global co-ordinate system of the plate by the θ ply orientation angle.

The stiffness matrices in equation (14) are found by integrating the ply contributions through the thickness of the plate

$$[A_{ij}] = \sum_{k=1}^N [\bar{Q}]_k (z_k - z_{k-1}) \quad (20)$$

$$[B_{ij}] = \frac{1}{2} \sum_{k=1}^N [\bar{Q}]_k (z_k^2 - z_{k-1}^2) \quad (21)$$

$$[D_{ij}] = \frac{1}{3} \sum_{k=1}^N [\bar{Q}]_k (z_k^3 - z_{k-1}^3) \quad (22)$$

where $[\bar{Q}]$ is the ply elasticity matrix in global co-ordinates (x, y, z) .

For simplifying the derivation the equations are given for a symmetrical balanced multi-layered composite lifting surface. It may be pointed out that this does not limit the proposed approach to symmetrical composites.

The strain and kinetic energies of the composite lifting surface can be written as follows, in case of no in-plane deformations:

$$V = \frac{1}{2} \int \int \int (\sigma_x \varepsilon_x + \sigma_y \varepsilon_y + \sigma_{xy} \varepsilon_{xy}) dx dy dz \quad (23)$$

$$T = \frac{1}{2} \int_0^t \int_{-b}^b \left(\frac{\partial \zeta}{\partial t} \right)^2 \rho dx dy \quad (24)$$

where ρ is the material density.

Present study uses Rayleigh–Ritz method to obtain free vibration, flutter, and divergence frequencies of lifting surfaces constructed of isotropic and advanced composite materials. Considering that the assumed functions are suitably chosen, this method provides not only the approximate value of the fundamental frequency, but also the approximate values at higher frequencies and mode shapes. An arbitrary number of functions can be used, and the number of frequencies that can be obtained is equal to the numbers of functions used. In this study in case of Rayleigh–Ritz nine modes are used. This number was achieved from convergence studies conducted on composite plates [14].

The derivation of the equations of motion for flutter-type aeroelastic instabilities is most conveniently obtained through the use of Hamilton's principle. Employing Hamilton's principle for a non-conservative elastic system would result in the following variational form that governs the dynamics of the system:

$$\delta \int_{t_1}^{t_2} L dt + \int_{t_1}^{t_2} \delta W_{nc} dt = 0 \quad (1c)$$

where L is the Lagrangian defined as $L = T - U$, T the total kinetic energy, U total potential or strain energy, δW_{nc} the virtual work done by the non-conservative forces—for this study it is the work done by aerodynamic forces—and t_1 and t_2 the initial and final time of the motion, respectively.

The assumed deflected shape is approximated by using an arbitrary number of functions. The number of functions chosen is equal to the number of modes that will be calculated. Even if only

the first few modes would be of most interest for flutter analysis, increasing the number of functions makes these modes more accurate. The modes and frequencies must converge at a certain value. To determine an accurate number of assumed functions, a free vibration analysis is performed by using nine modes. The out-of-plane deflection of the plate in generalized co-ordinates is expressed as follows:

$$\zeta(x, y, t) = \sum_{i=1}^N \gamma_i(x, y) \cdot q_i(t) \quad (25)$$

where $q_i(t)$ is the generalized displacement of the i th mode, and $\gamma_i(x, y)$ is as follows:

$$\gamma_i(x, y) = \Phi_i(x) \cdot \Psi_i(y) \quad (26)$$

Three types of deformation mode shapes can be quantified; namely, span-wise bending and torsion using built-in/free boundary conditions, and chordwise bending using free/free boundary conditions. These are represented analytically by following orthogonal functions:

$$\begin{aligned} \Phi_{Bn}(x) &= C_n [\sin \beta_2 x - \sinh \beta_2 x - \alpha_n (\cos \beta_n x - \cosh \beta_n x)] \\ \Psi_{Bn}(y) &= 1 \quad n = 1, \dots \\ \Phi_{Tm}(x) &= C_m \left(\sin \frac{(2m-1)\pi y}{2L} \right) \\ \Psi_{Tm}(y) &= \frac{1}{2} \left(1 - \frac{2y}{C} \right) \\ \Phi_{Ct}(x) &= \frac{C_k x}{L} \left(1 - \frac{x}{L} \right) \quad t = 1, 2, \dots \\ \Psi_{Ct}(y) &= [\sin \beta_k y + \sinh \beta_k y + \alpha_k (\cos \beta_k y + \cosh \beta_k y)] \end{aligned} \quad (27)$$

where β_n , α_n , β_k and α_k are the mode shape function coefficients, L is the lifting surface span, n number of bending modes used, m number of span-wise bending modes used, and t is the number of chordwise bending modes used.

Use of the Lagrange's equations yields the stiffness and mass matrix. Final forms of these matrices are given in Appendix.

When finite element method by discretization of Hamilton's Principle is used, the elements are taken from the Gradient Adaptive Transfinite Elements (GATE) Family [9]. These elements are formulated by combining blending-function method with transfinite interpolations. These transfinite elements differ from conventional elements in that it matches a given function on every point along the boundary for 2-D and over the surface for 3-D elements rather than on a finite number of points. A 16 d.o.f. and a 24 d.o.f. plate bending elements from the GATE family are utilized here for aeroelastic instability predictions. In the GATE family, the approximations can be in terms of either field variable, geometry variable and material variable or all of the variables.

The 16 degrees of freedom rectangular element has at each of the four corner nodes the displacement and its first normal derivatives and the cross derivative term as degrees of freedom. The 24 d.o.f. element contains additional second derivative terms as d.o.f. The elements of GATE

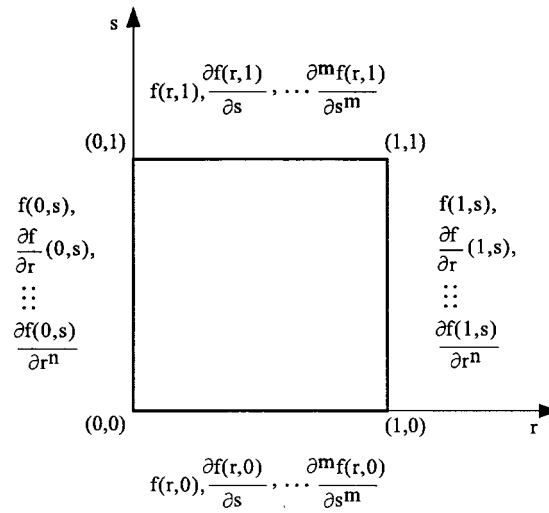


Figure 5. GATE family elements interpolation functions in 2-D

family are formulated within $[0, 1] \times [0, 1]$ bi-unit domain by defining projector operators in two perpendicular directions and using the Boolean sum which is the maximum operator. The approximate functions are obtained such that the function and the derivatives of the function up to a desired order with respect to r and s are continuous along the boundaries, Figure 5. The conventional finite elements are constructed by using the minimum operator, the tensor product, and the GATE family by using the maximum operator, the Boolean sum, as depicted in Figure 6.

For example, to formulate the 16 d.o.f. element, let a continuous function of two independent variables r and s be denoted by $f(r, s)$. Then, the r -direction projector operator for this element is

$$P_r[f] = \sum_{i=1}^1 \left[f(i, s) bf_{(i+1)}(r) + \frac{\partial f(i, s)}{\partial r} \cdot \frac{\partial bf_{(i+1)}(r)}{\partial r} \right] \tag{28}$$

and the s -direction projector operator is

$$P_s[f] = \sum_{i=0}^1 \left[f(r, i) bf_{(i+3)}(s) + \frac{\partial f(r, i)}{\partial s} \cdot \frac{\partial bf_{(i+3)}(s)}{\partial s} \right] \tag{29}$$

where bf functions are called ‘Blending Functions’.

The algebraically best approximation to f in 2-D is provided by the Boolean sum of these projectors P_r and P_s and is used in formulation of the GATE family of elements. The Boolean sum

$$f \simeq \bar{f} \equiv (P_r \oplus P_s)[f] = P_r[f] + P_s[f] - P_r P_s[f] \tag{30}$$

where $P_r P_s$ is the familiar tensor product used in conventional finite element formulations.

One other feature of the GATE family elements is that geometry and material property approximations are also obtained by using the Boolean sum. Complex geometries of advanced aerospace vehicles and material property changes due to aerodynamic heating can readily be

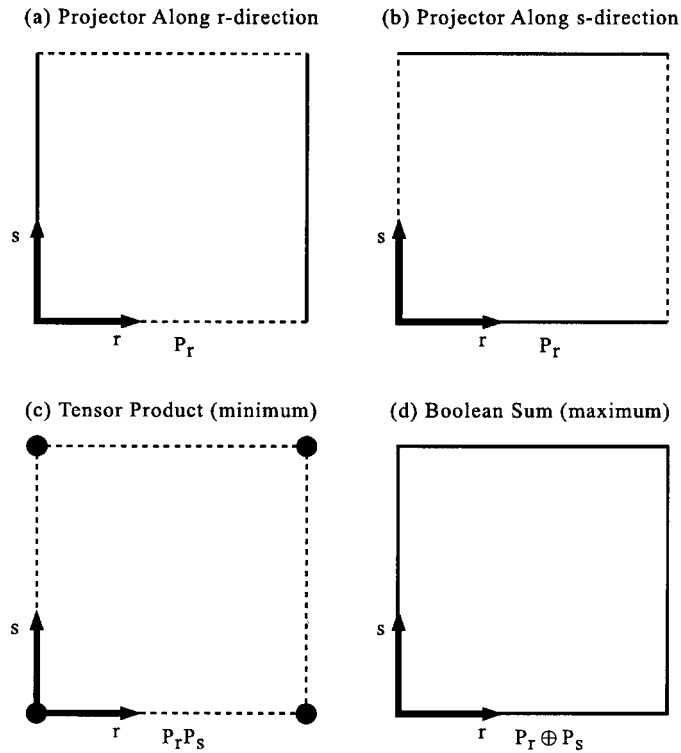


Figure 6. Boolean sum, tensor product and projectors

incorporated into the finite elements. The geometry and the field variables approximations take the form given below

$$x \simeq \bar{x} \equiv P_r[x] \oplus P_s[x] \oplus P_t[x] = \sum_{i=1}^{\text{NGDOF}} \text{NGEO}_i \cdot x_i \quad (31)$$

where NGEO_i is the geometry shape functions

$$E(r, s, t) \cong \bar{E}(r, s, t) \equiv P_r[E] + P_s[E] + P_t[E] = \sum_{i=1}^{\text{NMDOF}} \text{NMAT}_i \cdot E_i \quad (32)$$

where E shows a material constant, NMAT_i 's show the 'material shape functions', and NMDOF indicates the total number of element material degrees of freedom.

FLUID AND STRUCTURE INTERACTION MODEL

At the fluid and structure interface, the structural deformation and aerodynamic load transfer are achieved by using a meshless approach. Meshless method is a method in which the

approximating function is described in terms of nodes and a geometry of the domain as detailed by Belytschko [7].

In order to simplify the derivations following equations are based on 2-D model given in Figure 2. Given a set of nodes y_1, \dots, y_N and a set of nodal deformations (could include derivatives) d_1, \dots, d_N we want to approximate the original function $d(y_I) = d_I$. An approximation to deformation function d can be written as

$$d \simeq \bar{d} = p^T(y) \cdot a(y) = \sum_{i=1}^r p_i(y) \cdot a_i(y) \quad (33)$$

where p is a polynomial basis and a is a set of coefficients that will be determined. These coefficients $a(y)$ are then calculated by using an error minimization on the residual:

$$R = \sum_{I=1}^N W_I(y - y_I) (p^T(y_I) \cdot a(y) - d_I)^2 \quad (34)$$

where W_I is the weight function for node I . In this research cubic splines are used as the weight functions. Minimization of R with respect to a in equation (34) yields with a set of algebraic equations and then $a(y)$ coefficients can be calculated. As a result an approximation to d is obtained from equation (33).

In order to correctly predict induced loads due to structural deformations, in this research arbitrary out of plane deformations of the lifting surface, $\zeta_{\text{structure}}$ are mapped onto aerodynamic deformations, ζ_{aero}

$$\zeta_{\text{aero}}(x', y') = \mathfrak{J}[\zeta_{\text{structure}}(x, y)] \quad (35)$$

Depending on the flight velocities in question, different weighting functions are used. In this research, cosine functions from subsonic incompressible flow and uniform functions for supersonic and hypersonic flow are used as the weighting function. It may be noted that the transonic flight velocities are not included here, but this is not a limitation of the meshless approach.

This approach allows direct interfacing of the new developments from both the structure and the fluid for aeroelastic instability predictions without modifying the aeroelastic solution method.

FLOW MODEL AND SOLUTION METHODS

The unsteady flow is taken to be a small perturbation from the steady uniform flow over the equivalent flat plate lifting surface. Unsteady aerodynamic models for incompressible, subsonic, supersonic, and hypersonic flow are implemented in the AIM program for flutter and divergence type aeroelastic instability predictions.

For incompressible flow using thin airfoil assumptions, Theodorsen [15] and Spielberg [16] have derived relationships for unsteady aerodynamic lift and moment coefficients for rigid body bending, rigid body torsion, and parabolic deformation of the airfoil camber as a function of reduced frequency and elastic axis position when the airfoil oscillations are of simple harmonic of $\exp(i\omega t)$. These are given in Appendix for completeness. While these analytical relationships are extremely useful, they restrict the type of vibratory deformations that can be considered.

In order to expand the range of unsteady vibratory motions that can be analysed, the Kernel Function approach is used. In this approach the governing equations of fluid mechanics for two-dimensional flow are re-cast into an integral equation of the form given below

$$\bar{w}(y) = \omega \int_{-c/2}^{c/2} \frac{\Delta \bar{p}(\xi)}{\rho_{\infty} U^2} K_A \left(\frac{2k(y - \xi)}{c} \right) d\xi \quad (36)$$

$K_A(y_0)$ is the Kernel function which represents the upwash at the y location due to a unit pressure pulse at the ξ location. For linearized thin airfoil theory, the upwash velocity along the chord of the lifting surface for simple harmonic motion is given by

$$\bar{w}(y) = U \left[2ki \frac{\bar{\xi}}{c} + \frac{\partial \bar{\xi}}{\partial y} \right] \quad (37)$$

For simple harmonic motion, the Kernel function $K_A(y_0)$, for incompressible irrotational two-dimensional flow is

$$K_A(y_0) = \frac{1}{2\pi} \left\{ i e^{-iy_0} \left[\text{Ci}(y_0) + i \left[\frac{\pi}{2} + \text{Si}(y_0) \right] - \frac{1}{y_0} \right] \right\} \quad (38)$$

where $\text{Ci}(y_0)$ and $\text{Si}(y_0)$ represent the cosine and sine integral functions, respectively.

There are many classical solution methods available for the solution of this type of integral equation. In this research a standard algebraic method is used. It may be noted that there is a difficulty since this Kernel Function contains singularities of the form $1/y_0$ and $\ln(y_0)$; the $\ln(y_0)$ appears in the cosine integral term. The $1/y_0$ singularity is handled by making the integration points, ξ , different from the collocation points, y . The $\ln(y_0)$ singularity is addressed by using the method given by Whitehead [17].

For a selected discretization of the airfoil in terms of y and ξ and using trapezoidal rule weighting for the integration, a matrix statement results

$$\{\bar{w}\} = [K_A][D] \left\{ \frac{\Delta \bar{P}}{\rho_{\infty} U^2} \right\} \quad (39)$$

The unknown chordwise distribution of the unsteady pressure coefficient $\{\Delta \bar{p}/\rho_{\infty} U^2\}$ is then determined through matrix inversion. Any number of upwash functions can be used and the unsteady pressure coefficient is found for each one from the multiplication of the inverse of the Kernel Function and weighting matrix times the upwash velocity matrix, as given below:

$$\left\{ \frac{\Delta \bar{P}}{\rho_{\infty} U^2} \right\} = [[K_A][D]]^{-1} \{\bar{w}\} \quad (40)$$

For hypersonic flow the so-called piston theory approach (see for example [18]) presented by Lighthill can be used as opposed to full potential flow solution. In this approach the pressure acting on the surface is equivalent to the pressure acting on a piston in a tube. This leads to a simple relationship between the upwash and unsteady pressure on the surface of the vibrating lifting surface.

As stated in a recent paper the piston theory may be acceptable in the moderately high Mach number range; however, caution must be exercised for $M = 1.2$ and also $M =$ over 20 flight velocities [19]. This is due to the strong wave/shock interaction effects. Therefore, the numerical examples presented in here do not cover the above-mentioned Mach numbers.

In piston theory, for a flat plate, the change in pressure across the lifting surface is represented as

$$\Delta\bar{P}(y) = -2\rho_\infty a_\infty \bar{w}(y) \quad (41)$$

where $\bar{w}(y)$ is the upwash and is given by

$$\bar{w}(y) = \partial\bar{\zeta}/\partial t + U(\partial\bar{\zeta}/\partial x) \quad (42)$$

As it is seen the piston velocity includes a convection term $U(\partial\bar{\zeta}/\partial x)$ as well as a direct velocity term $\partial\bar{\zeta}/\partial t$.

Given a selected discretization of the airfoil in terms of y , the unknown chordwise distribution of unsteady pressure ($\Delta\bar{P}$) is determined for any of these unsteady aerodynamic models. Any number of upwash functions can be used and the unsteady pressure difference is found for each one. Once the unsteady chordwise pressure difference is determined, the generalized aerodynamic force can be calculated.

The expression for the generalized unsteady aerodynamic force has the term

$$Q_a(t) = \pi\rho_\infty b^2 [M_a] \{\ddot{q}\} + 2\pi\rho_\infty U^2 [C_a] \{\dot{q}\} + \pi\rho_\infty U^2 [K_a] \{q\} \quad (43)$$

The aerodynamic mass, $[M_a]$, damping $[C_a]$, and stiffness $[K_a]$ matrices are determined from the unsteady chordwise pressure distribution. When a harmonic motion is assumed the generalized displacements can be expressed as

$$\{q\} = \{\bar{q}\} e^{i\omega t} \quad (44)$$

Substituting equation (32) into equation (31) and solving for U from the reduced frequency definition $U = \omega b/k$ gives the generalized aerodynamic force as

$$Q_1(t) = \pi\rho_\infty \omega^2 b^3 e^{i\omega t} \sum_{i=1}^n \bar{A}_{ij} \bar{q}_j \quad (45)$$

where \bar{A}_{ij} 's are the elements of the $n \times n$ complex-valued aerodynamic influence matrix.

NUMERICAL EXAMPLES

In order to illustrate the practical applications of the efficient procedures developed, flutter and divergence type aeroelastic instability predictions of representative lifting surfaces are presented in this section. Mach numbers selected represent flow conditions ranging from subsonic, supersonic, and hypersonic.

Parametric study of composite lifting surface

Flutter and divergence velocities are computed for a multi-layered T300/5208 graphite epoxy lifting surface by varying the aspect ratio and ply orientation angle. For this parametric study,

flight conditions were taken to be subsonic at 9000 m. The structure was modelled as an equivalent plate using Rayleigh–Ritz with eight (four bending and four torsional), and nine (four bending, four torsional, and one chordwise bending) modes in order to see the effects of chordwise bending modes on aeroelastic instability modes. Flow is modelled by using thin airfoil assumptions first using lift and moment coefficients given in Appendix and then using Kernel functions. The entire range of $-90^\circ < \theta < 90^\circ$ of $[\pm \theta/0]_s$ balanced laminate lifting surface with structural Aspect Ratio (AR) of up to 8. Results compared well with experimental values available at certain angles [14].

While the low aspect ratio lifting surfaces have torsional and chordwise bending or the coupling of these two as flutter modes, higher aspect ratio lifting surfaces have span-wise bending or torsion or bending-torsion coupled flutter modes. The inclusion of Chordwise Vibration Mode (CVM) affects both low and high aspect ratio lifting surfaces. With CVM included, a better convergence is obtained regardless of the aspect ratio. For low aspect ratio lifting surfaces CVM itself could become the flutter mode or be coupled with torsion mode. In this case, exclusion of this prevents not only the good convergence, but also the prediction of flutter mode within the flight envelope. Figure 7 depicts U - g diagram for aspect ratio of 8 lifting surface. With inclusion of chordwise effects, predicted flutter speed is 8 per cent lower and the flutter type remains as first torsion.

The divergence velocities showed an opposite trend to flutter. It was observed that $[\pm \theta/0]_s$ laminate exhibited always first bending as divergence mode when there is one. The first bending mode is usually a very fast converging mode and not influenced by the inclusion of CVM. However, portions between $-90^\circ < \theta < -45^\circ$ and $75^\circ < \theta < 90^\circ$ are affected by the inclusion of CVM (Figure 8). Figure 9 illustrates the change of flutter speed as the aspect ratio increases. Another point that may be useful to the designer is that divergence might be eliminated for a certain range of $[\pm \theta/0]_s$ laminates, and for high aspect ratio lifting surfaces divergence free region widens as can be seen from Figure 10.

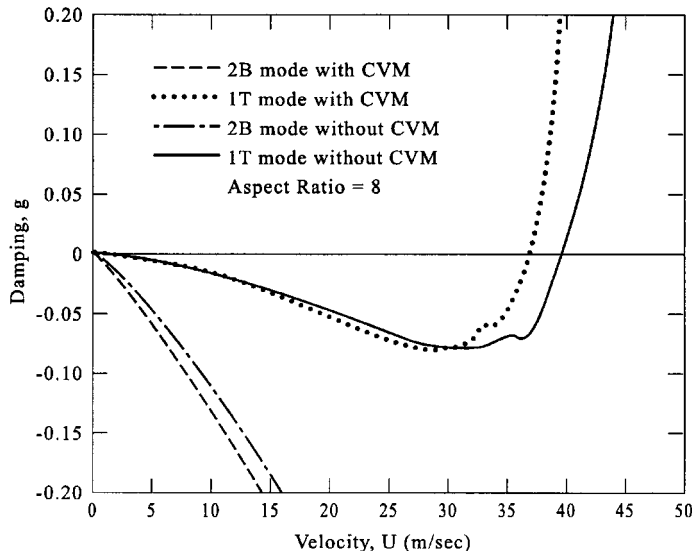


Figure 7. U - g diagram for $[\pm 60/0]_s$ balanced laminate, AR = 8

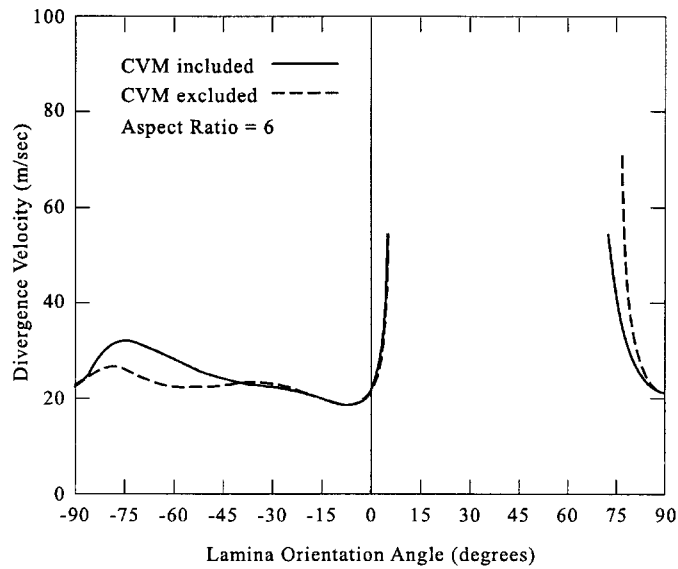


Figure 8. Effect of chordwise vibration modes on divergence as a function of ply angle, AR = 6

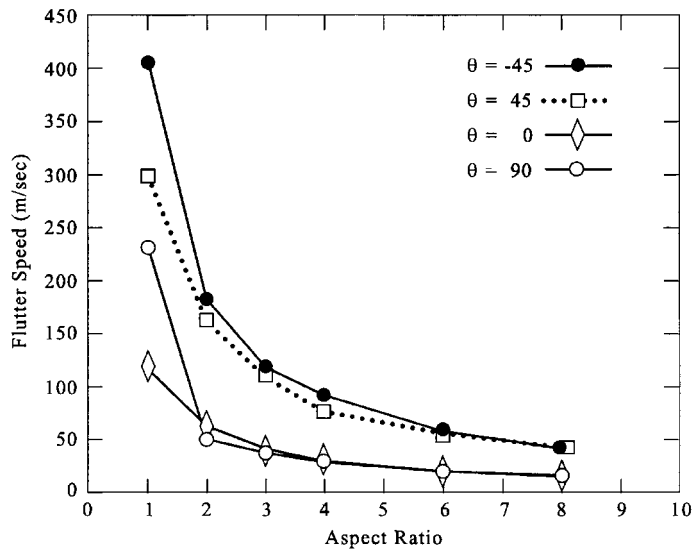


Figure 9. Flutter velocity versus aspect ratio for various θ values of $[\pm \theta/0]_s$ laminate

Effects of chordwise modes on supersonic flight

A T300/5208 graphite epoxy equivalent flat plate lifting surface is studied to see the effects of inclusion of chordwise bending modes in Rayleigh–Ritz analysis. For this study the structural

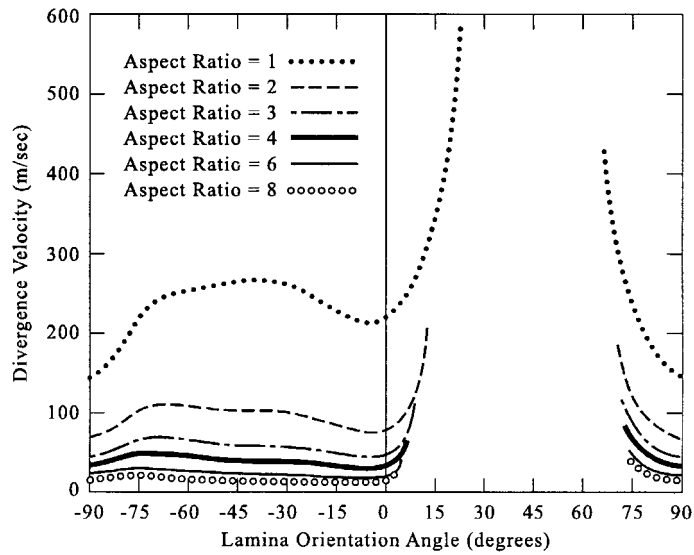


Figure 10. Divergence velocity versus entire angle range of $[\pm \theta/0]_s$ laminate (AR = 1 to 8)

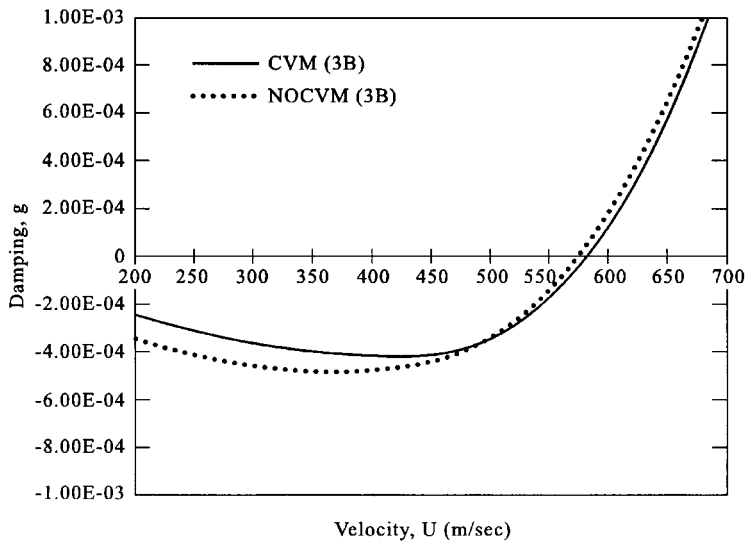


Figure 11. $U-g$ diagram for $[+ 30/0]_s$ balanced lifting surface (AR = 8, Altitude = 9 km, thickness = 0.007 m, $M = 2.5$)

aspect ratio was 8, the thickness was 0.007 m and the Mach number was 2.5 at 9 km. It is seen that the flutter mode stayed as the third bending and flutter velocity is increased by addition of the chordwise modes. Small change in flutter velocity is due to the fact that the aspect ratio is large, Figure 11.

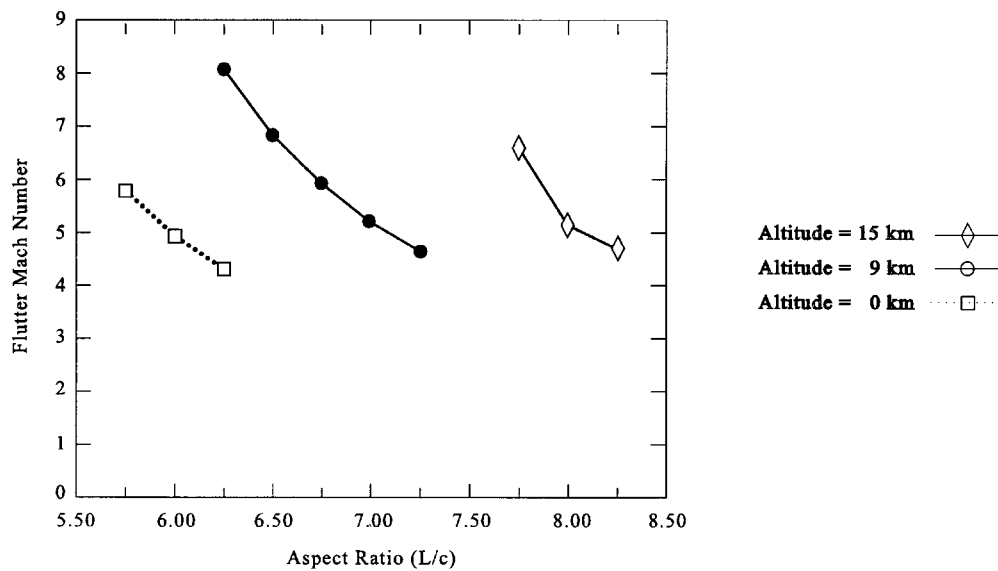


Figure 12. Hypersonic flutter mach number versus lifting surface aspect ratio for altitudes 0, 9 and 15 km ($h/c = 0.02$, Inconel x-750)

Effects of lifting surface aspect ratio on hypersonic flutter

An Inconel x-750 lifting surface is modelled as an equivalent plate of thickness-to-chord ratio 0.02. Flight conditions at 0, 9, and 15 km are taken and flutter velocities are calculated as a function of lifting surface structural aspect ratio. For flutter predictions finite elements for the structure and Kernel functions for the flow are used. It is observed that as the aspect ratio increases, flutter velocity is decreased at all flight conditions, Figure 12.

Aerodynamic heating effects on flutter

This is to simulate the structural stiffness loss effects at high velocity flow due to aerodynamic heating. For this purpose two lifting surfaces are studied made of a super alloy Inconel x-750 and composite carbon-carbon.

For the Inconel x-750 lifting surface, elevated temperature effects are studied for Mach numbers 4 to 10. Temperature effects are simulated by using material properties at elevated temperatures and calculation of structural deformations based on that. It is seen as depicted in Figure 13 that flutter velocity decreased with elevated temperatures.

For a carbon-carbon lifting surface, aerodynamic heating effects are simulated as being 4500° F. Mach numbers varied from 4 to 30 in this case. It is seen that flutter velocity is decreased with aerodynamic heating. But, the rate of the flutter velocity decrease reduces beyond Mach 18 as depicted in Figure 14. This could be due to the fact that the piston theory is not accurate beyond Mach 20 [19].

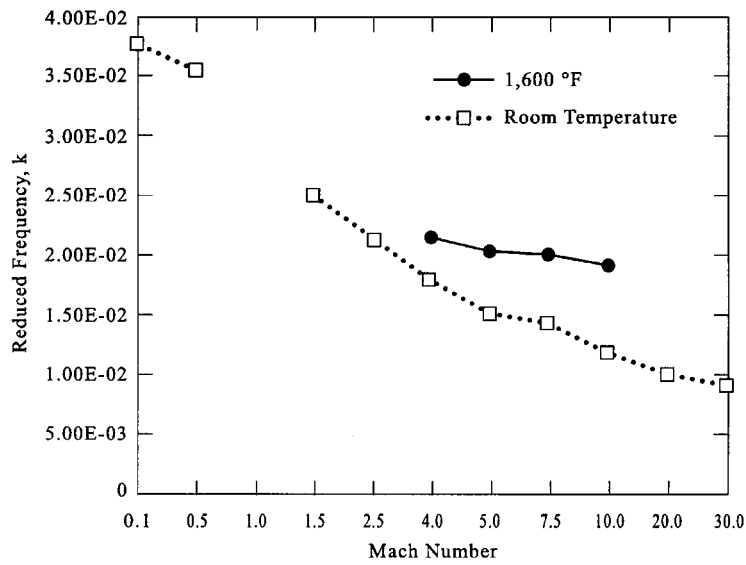


Figure 13. Effect of aerodynamic heating on flutter reduced frequency of inconel x-750 lifting surface (AR = 8, $h/c = 0.016$, altitude = 9 km)

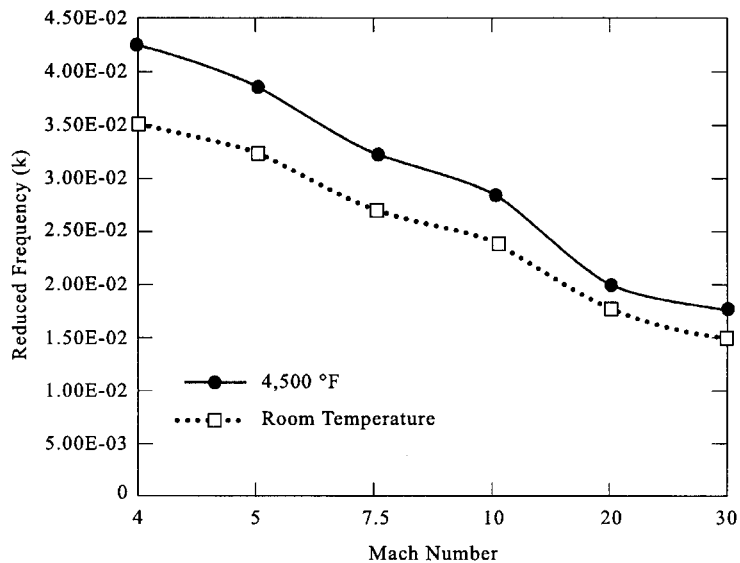


Figure 14. Effect of aerodynamic heating on flutter reduced frequency of carbon-carbon lifting surface (AR = 8, $h/c = 0.016$, altitude = 9 km)

Equivalent plate thickness/chord ratio and flutter velocity

An aluminum alloy lifting surface is simulated as an equivalent thin plate of Aspect Ratio 8. Flight conditions are at 0, 9, and 15 km subsonic, supersonic, and hypersonic. The plate thickness

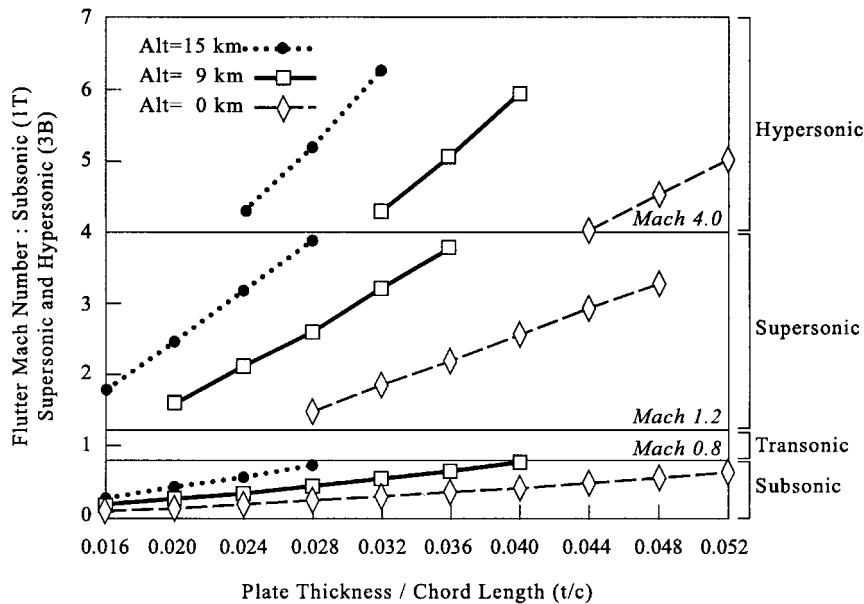


Figure 15. Flutter Mach number as a function of lifting surface equivalent thickness/chord length, Aluminium alloy, AR = 8. (Variables: Altitude—0, 9, 15 km; Flight regime—subsonic, supersonic, hypersonic)

to chord length ratio is varied and flutter Mach numbers are obtained, Figure 15. At certain thickness ratios, flutter is avoided at different flight velocities. At the preliminary design sizing this information could be helpful.

CONCLUDING REMARKS

Meshless Methods, Finite Elements, Rayleigh–Ritz, and Kernel Functions are used to develop an efficient procedure for multidisciplinary computation of fluid and structure interaction problems of aerospace vehicles. Although the actual computing times could not be compared for each parametric study, with the present approach each example was solved in less than ten minutes using an average speed work station. This could be attributed to usage of meshless methods together with high accurate finite elements.

The multidisciplinary approach presented here is advantageous since

- (1) it is efficient and can be incorporated into design iterations,
- (2) it uses meshless approach and therefore any new developments from structure or flow solution methods can readily be incorporated in aeroelastic instability predictions.

Finally, numerical examples presented should be helpful in preliminary design stage of aerospace vehicles with lifting surfaces of advanced materials as well as traditional isotropic materials.

APPENDIX

Elements of $[M]$, $[K]$ and $[A]$ matrices for bending – torsion-chordwise bending coupled composite laminate using Rayleigh–Ritz approach with Theodorsen [15] and Spielberg [16] unsteady aerodynamic coefficient,

$$M_{BB} = \int_0^L \int_0^c \Phi_B^2 \Psi_B^2 dx dy$$

$$M_{TT} = \int_0^L \int_0^c \Phi_T^2 \Psi_B^2 dx dy$$

$$M_{CC} = \int_0^L \int_0^c \Phi_C^2 \Psi_T^2 dx dy$$

$$K_{TT} = \left[\frac{4D_{66}}{c} \int_0^L (\Phi_T')^2 dx \right] \left(\frac{k_n T}{(2n-1)\pi^{3/2}} \right)$$

$$K_{BT} = 2D_{16} \int_0^L \Phi_B'' \Phi_T' dx$$

$$K_{BC} = D_{12} \int_0^L \int_0^c \Phi_B'' \Phi_C \Psi_C'' dx dy$$

$$K_{TC} = 2D_{16} \int_0^L \int_0^c (\Phi_T'' \Phi_C' \Psi_T \Psi_C') dx dy + 2D_{26} \int_0^L \int_0^c \Phi_T' \Phi_C \Psi_T' \Psi_C'' dx dy$$

$$K_{CC} = D_{11} \int_0^L \int_0^c (\Phi_C'')^2 dx dy + D_{22} \int_0^L \int_0^c (\Phi_C)^2 (\Psi_C'')^2 dx dy$$

$$+ 4D_{66} \int_0^L \int_0^c (\Phi_C')^2 (\Psi_C')^2 dx dy$$

$$A_{BB} = L_A \frac{1}{6} \int_0^L \Phi_B^2 dx$$

$$A_{TT} = \frac{M_B}{4} \int_0^L \Phi_T^2 dx$$

$$A_{BT} = \frac{L_B}{c} \int_0^L \Phi_B \Phi_T dx$$

$$A_{TB} = \frac{M_A}{2} \int_0^L \Phi_T \Phi_B \, dx$$

$$A_{BC} = L_C \frac{1}{b} \int_0^L \Phi_B \Phi_C \, dx$$

$$A_{CB} = \frac{N_A}{b} \int_0^L \Phi_B \Phi_C \, dx$$

$$A_{TC} = \frac{M_C}{c} \int_0^L \Phi_T \Phi_C \, dx$$

$$A_{CT} = \frac{N_B}{c} \int_0^L \Phi_T \Phi_C \, dx$$

$$A_{CC} = N_C \frac{1}{b} \int_0^L \Phi_C^2 \, dx$$

where k_{nt} are structural aspect ratio corrections. The complex functions of $L_A, \dots, N_A, \dots, M_A$ can be found in [2].

ACKNOWLEDGEMENTS

The author would like to acknowledge her Ph.D. advisor Professor Richard H. Gallagher (1927–1997) for providing the author's first introduction to multidisciplinary research.

REFERENCES

1. Dowell EH, Curtiss HC, Scanlan RH, Sisto F. *A Modern Course in Aeroelasticity*. Sitsthoff & Nordhoff International Publishers: Alphen a/d Rijn, 1978.
2. Fung YC. *An Introduction to the Theory of Aeroelasticity*. Wiley: New York, 1955; 195–220.
3. Gallagher RH, Padlog J, Bijlaard PP. Stress analysis of heated complex shapes. *ARS Journal* 1962; **32**(5):700–707.
4. Thornton EA, Oden JT, Tworzydlo WW, Youn SK. Thermoviscoplastic analysis of hypersonic structures subjected to severe aerodynamic heating. *Journal of Aircraft* 1990; **27**(9):826–835.
5. Odabas OR, Sarigul-Klijn N. Thermomechanical coupling effects at high flight speeds. *AIAA Journal* 1994; **32**(2):425–430.
6. Sarigul-Klijn N, Sarigul N. Sonlu Elemenlarla Hesabin Esaslari (in Turkish) (Translation of Finite Element Analysis: Fundamentals by R. H. Gallagher) Prentice-Hall: Englewood Cliffs, NJ, 1994, ISBN, 0-9643757-0-2.
7. Belytschko T, Krongauz Y. Meshes methods: an overview and recent developments. *Computer Methods in Applied Mechanics and Engineering* 1996; **139**:3–47.
8. AIM: Aeroelastic Instability Modes Code, N. Sarigul-Klijn, 1996.
9. Sarigul-Klijn N. On the formulation of gradient adaptive transfinite elements (GATE) family, NSK, Davis, CA, 1997, ISBN 0-9643757-1-0.
10. Done GTS. Interpolation of mode shapes: a matrix scheme using two-way spline curves. *Aeronautical Quarterly* 1965; **16**:333–349.
11. ABAQUS User's Manual. Hibbit, Karlsson and Sorensen, Inc: RI, 1995.
12. Sarigul-Klijn N, Capece VR. Coupled fluid-structure instabilities at high flight speeds. *Proceedings of 10th International Conference on FEF*, 1998.
13. Jones RM. *Mechanics of Composite Materials*. McGraw-Hill: New York, 1992.
14. Sarigul-Klijn N, Oguz S. Effect of aspect ratio and ply orientation on aeroelastic response of composite plates. *Journal of Aircraft* 1998; **35**(4):657–659.

15. Theodorsen T. General theory of aerodynamic instability and the mechanism of flutter. NACA Report 496, (1935).
16. Spielberg IN. The two dimensional incompressible aerodynamic coefficients for oscillatory changes in airfoil camber. *Journal of Aeronautical Sciences*, 1953; **1**(6):432–436.
17. Whitehead DS. Force and moment coefficients for airfoils in cascade. British Reports and Memoranda No. 3254, 1960.
18. Ashley H, Zortarian G. Piston theory—a new aerodynamic tool for the aeroelastician. *Journal of Aeronautical Science*. 1956; **23**(12):1109–1118.
19. Chaves FR, Liu DD. Unsteady unified hypersonic/supersonic method for aeroelastic applications including shock/wave interaction. *AIAA Journal* 1995; **33**(6):1090–1097.